Interplay of noise and reservoir-induced decoherence in persistent currents

Samudra Sur* and Thierry Giamarchi
Department of Quantum Matter Physics, University of Geneva, Quai Ernest-Ansermet 24, 1211 Geneva, Switzerland

(Received 11 October 2025; accepted 12 September 2026; published 9 November 2026)

Persistent current is a hallmark of quantum phase coherence. We study the fate of the persistent current in a nonequilibrium setting, where a tight-binding ring is subjected to stochastic disorder as well as a fermionic reservoir attached to each site. We evaluate the current using the Keldysh technique and find that it exhibits nonmonotonic behavior, suggesting two distinct mechanisms of decoherence. While coupling to the reservoirs introduces a coherence length scale given by the inverse of the coupling strength, the other mechanism is more subtle and driven by the ratio of noise strength to reservoir coupling. The interplay of noise and reservoir constitutes a purely nonequilibrium steady state with a flatter distribution function that we effectively describe using classical rate equations. We also discuss possibilities of realizing our findings in ultracold-atom experiments.

DOI: 10.1103/486b-4qgc

I. INTRODUCTION

Decoherence or loss of quantum coherence is ubiquitous as quantum many-body systems are never perfectly isolated. Interaction with the environment [1–4], presence of noise [3–6], and quantum measurements [7–15] lead to loss of coherence, giving rise to emergent classical behavior. On the contrary, isolated disordered systems in equilibrium may undergo intrinsic decoherence due to electron-electron or electron-phonon interaction, resulting in suppression of interference effects like weak localization [16–18] and persistent current (PC).

Persistent current is one of the striking signatures of quantum phase coherence, arising when electronic wavefunctions remain coherent around a mesoscopic ring threaded by magnetic flux, producing the Aharonov-Bohm effect. Consequently, a suppression of the current indicates that one or several mechanisms of decoherence are at play. Although first introduced in early quantum mechanics [19], persistent currents gained significant attention only after their modern formulation in the context of mesoscopic systems [20]. Over the last few decades, both analytical [21–39] and numerical [40–44] studies have elucidated the role of static impurities, interactions, and temperature on the PC. Several experimental works [45–50] on isolated and ensembles of small metal rings have confirmed these understandings. Beyond fundamental interests, PC in ultracold atomic rings has also found applications [51,52] in high-precision rotation sensing, atomtronic superconducting quantum interference device (SQUID) analogs for flux detection, and neutral persistent-current qubits.

While PC has been studied in the context of systems in thermodynamic equilibrium and in the presence of electron reservoirs [35–37], its behavior in nonequilibrium systems driven by the interplay of stochastic noise and reservoir coupling remains elusive. Such an interplay is known to give rise to nonequilibrium steady states [53–62] marked by unusual transport [63–76], dephasing [76–81] and entanglement [7,8,82–87] properties. In such systems, PC can reveal the decoherence mechanisms due to the competing effects of noise and reservoir coupling. Moreover, considering the averaged dynamics, due to a correspondence between such stochastic systems and quantum systems under continuous weak measurements [14,88–90] through a process known as *unraveling* [91–94], PC can also probe the decoherence processes in weakly yet continuously monitored systems.

In this paper, we investigate the decoherence mechanisms that result in the decay of the persistent current in a ring of fermions subjected to stochastic white noise and fermionic reservoirs coupled to each site. Using a Keldysh formalism [95], we find that noise and reservoir effects compete rather than add, giving rise to two distinct decoherence mechanisms exhibiting unusual decay of PC. Remarkably, the reservoirs play a dual role, with weak coupling supporting the current while strong coupling suppressing it. In the context of continuously monitored systems, the same mechanisms would prevail with noise strength replaced by the measurement rate.

The rest of the paper is organized as follows. In Sec. II, we introduce the model of our study and also quantitatively define persistent current. In Sec. III, we introduce the Keldysh action to describe the nonequilibrium system, compute the effective contribution of the fermionic reservoirs, and also derive the effective action by performing the disorder averaging. In Sec. IV, we discuss the self-energy induced by the stochastic noise and compute exact expressions for the full nonequilibrium Green's functions of the system with the help of self-consistent Born method. In Sec. V, we calculate the steady-state persistent current and show that it shows nonmonotonic behavior due to two decoherence mechanisms.

*Contact author: samudra.sur@unige.ch

Published by the American Physical Society under the terms of the Creative Commons Attribution 4.0 International license. Further distribution of this work must maintain attribution to the author(s) and the published article's title, journal citation, and DOI.

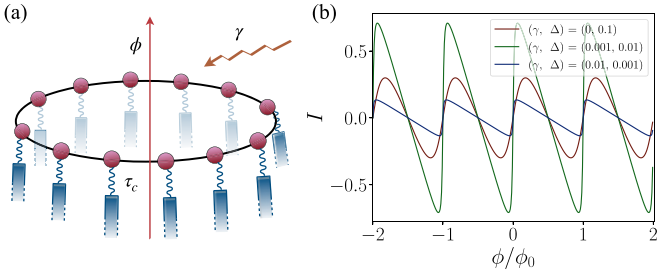


FIG. 1. (a) Schematic of the tight-binding ring in the presence of a time-dependent stochastic noise with strength γ and identical one-dimensional fermionic reservoirs coupled to each site with coupling strength τ_c. The ring is threaded by a magnetic flux ϕ that gives rise to the persistent current in the system. (b) Persistent current in units of $I_0 = ev_F/L$ as a function of flux ϕ/ϕ_0 for three different sets of $(\gamma, \Delta) = (0, 0.1), (0.001, 0.01), (0.01, 0.001)$ in the units of t. Δ : bath hybridization function (see main text). The system size is $L = 16$ with $N = 8$ electrons.

Then, in Sec. VI we describe the two decoherence mechanisms in detail. Finally, in Sec. VII we summarize and provide future perspectives. Some of the details of the calculations are provided in the Appendixes.

II. THE MODEL: NOISY RING

We consider a tight-binding ring of spinless fermions on L sites, subjected to a stochastic disorder that couples to the fermion density. Identical fermionic reservoirs with an energy dispersion E_q, chemical potential μ, and temperature T are connected to every site, which helps maintain a steady state in the presence of noise. As the ring is threaded by a magnetic flux ϕ, the Hamiltonian of the composite system is given by

$$\begin{aligned} H(t) = & -t\sum_{j=1}^{L}(e^{ieA}\psi_j^\dagger\psi_{j+1} + \text{H.c.}) + \sum_{j=1}^{L} V_j(t)\psi_j^\dagger\psi_j \\ & + \sum_{i=1}^{L}\sum_{q}(E_q - \mu)c_{q,j}^\dagger c_{q,j} \\ & - \tau_c\sum_{j=1}^{L}\sum_{q}(\psi_j^\dagger c_{q,j} + \text{H.c.}). \end{aligned} \tag{1}$$

The ring fermion (ψ_j) at site j is coupled to the zeroth site of the corresponding reservoir ($c_{r=0,j} = \sum_q c_{q,j}$) with coupling strength τ_c, while the tight-binding hopping in the ring is given by t. The magnetic flux is incorporated as a vector potential $A = \frac{2\pi}{L}(\phi/\phi_0)$, where ϕ_0 is the flux quantum and $\hbar$ has been set to 1 for convenience. The stochastic disorder $V_j(t)$ is a Gaussian white noise, with the noise correlation given by

$$\overline{V_i(t)V_j(t')} = 2\gamma\ \delta_{ij}\delta(t - t'). \tag{2}$$

A schematic of the model is shown in Fig. 1(a) for illustration. The total persistent current in the presence of magnetic flux is given as a weighted sum over the energy levels $I(\phi) = \sum_n f(\mathcal{E}_n(\phi))I_n(\phi)$, where $f(\mathcal{E})$ is the distribution function and

$$I_n(\phi) = -\frac{e}{L}\frac{\partial\mathcal{E}_n(\phi)}{\partial k_n} = -ev_n(\phi)/L \tag{3}$$

is the current carried by nth energy level [22] in the presence of flux. For a system in thermal equilibrium, $f(\mathcal{E})$ would be given by the Fermi-Dirac distribution. Evidently, in a system with translational invariance, the net PC would be zero in the absence of magnetic flux, due to the exact cancellation of the currents carried by the pair of levels at k and $-k$. However, the presence of a magnetic flux (noninteger multiple of ϕ_0) breaks the time-reversal symmetry, thereby generating a nonzero PC.

III. KELDYSH ACTION

To study the nonequilibrium steady state due to the interplay of these two effects, we start with the Keldysh partition function [95] given by

$$Z = \int \mathcal{D}(\bar\psi, \psi)\int \mathcal{D}(\bar c, c)e^{iS(\bar\psi,\psi,\bar c,c)}, \tag{4}$$

where the Keldysh action S can be split into parts involving the system (s), bath (b), and coupling (s-b), i.e.,

$$S = S_s(\bar\psi, \psi) + S_b(\bar c, c) + S_{s\text{-}b}(\bar\psi, \psi, \bar c, c). \tag{5}$$

We assume that the Grassmann fields $(\bar\psi, \psi, \bar c, c)$, defined on the upper and lower branches of the Keldysh contour, have been rotated following Larkin-Ovchinnikov (LO) prescription [96]. The quadratic nature of S_b and $S_{s\text{-}b}$ allows us to integrate out the reservoir fermions and incorporate it as an effective term in S_s. In Fourier space, we perform the Gaussian integral involving the reservoir fermions, assuming a constant density of states (DOS) (the details of this derivation are provided in Appendix A). This yields finally $S = S_s + S'(\bar\psi, \psi)$, where

$$S' = i\Delta\iint\frac{d\omega}{2\pi}\frac{dk}{2\pi}(\bar\psi^1\quad\bar\psi^2)\begin{pmatrix}1 & 2\tanh\left[\frac{\omega-\mu}{2T}\right]\\ 0 & -1\end{pmatrix}\begin{pmatrix}\psi^1\\ \psi^2\end{pmatrix}. \tag{6}$$

The superscripts 1 and 2 denote the LO rotated Grassmann fields in Keldysh space, and we have omitted the k, ω labels for the fields for brevity. Furthermore, we introduce $\Delta = \tau_c^2/\mathrm{v}_F$, the bath hybridization function. Here, v_F, the Fermi velocity of the reservoir, is directly related to the constant DOS of the reservoir per unit length as $\rho_0 = 1/(\pi\mathrm{v}_F)$. The resulting full action can yet again be separated into two parts, $S = S_0 + S_{\text{dis}}$, where S_0 governs the nondisordered part of the ring incorporating the effect of the reservoirs and S_{dis} describes the stochastic noise. The advantage of such separation is that the former, being time independent and quadratic, can be expressed in terms of exact retarded, advanced, and Keldysh Green's functions $g_{R/A/K}$. The entire procedure of integrating out the reservoirs amounts to the appearance of a finite lifetime and a temperature in the Green's functions of the ring fermions. More specifically, S_0 is given by

$$S_0 = \int\frac{d\omega}{2\pi}\int\frac{dk}{2\pi}(\bar\psi^1\quad\bar\psi^2)\begin{pmatrix}g_R^{-1} & [g^{-1}]_K\\ 0 & g_A^{-1}\end{pmatrix}\begin{pmatrix}\psi^1\\ \psi^2\end{pmatrix}, \tag{7}$$

with $g_{R(A)}^{-1} = \omega - \mathcal{E}(k) \pm i\Delta$ and $[g^{-1}]_K = 2i\Delta\tanh(\frac{\omega-\mu}{2T})$.

Heuristically, the bath hybridization Δ can now be understood as the effective imaginary self-energy of an electron going from the ring to the reservoir and back. Naturally, this suggests that an electron in the ring has a finite lifetime given by the inverse of Δ due to the presence of reservoirs.

The disorder averaging over the Gaussian distribution is performed at the level of the Keldysh partition function. In Fourier space, the probability distribution for the disorder potential can be expressed as $P[V] = \exp[-\frac{1}{4\gamma}\int\frac{dk}{2\pi}\int\frac{d\omega}{2\pi}V^*(k,\omega)V(k,\omega)]$, $V(k,\omega)$ being the Fourier transform of $V_i(t)$. The disorder averaging

$$\overline{Z} = \int \mathcal{D}(\bar{\psi},\psi)e^{iS_0}\int \mathcal{D}V P[V]e^{iS_{\rm dis}[V]}$$

gives rise to quartic terms in the action (see Appendix B for the detailed derivation):

$$\overline{Z} = \int \mathcal{D}(\bar{\psi},\psi)e^{iS_0}\exp\Big\{-\gamma\sum_j\int_{-\infty}^{\infty}dt\big(\bar{\psi}_j^1(t)\psi_j^1(t) + \bar{\psi}_j^2(t)\psi_j^2(t)\big)\big(\bar{\psi}_j^1(t)\psi_j^1(t)+\bar{\psi}_j^2(t)\psi_j^2(t)\big)\Big\}. \quad (8)$$

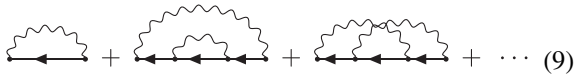
Note that, while the original action is not translationally invariant, disorder averaging with the given probability distribution restores the translational invariance.

IV. SELF-ENERGY: SELF-CONSISTENT BORN METHOD

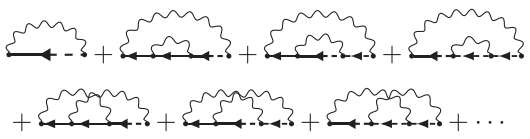
At the level of the Green's function, this effective *interaction* arising from the disorder averaging is incorporated through a self-energy $\mathbf{\Sigma}$. Subsequently, the Dyson equation $\mathbf{G} = [\boldsymbol{g}^{-1} - \mathbf{\Sigma}]^{-1}$ relates the full Green's function with the bare Green's function $\boldsymbol{g}$ and self-energy $\mathbf{\Sigma}$. The boldface indicates that it is a matrix equation with each quantity having 2×2 structure in Keldysh space. Diagrammatically, we represent the different components of $\boldsymbol{g}$ as follows:

$g_R =$, $g_A =$, $g_K =$

In general, the self-energy $\mathbf{\Sigma}$ is given as a series of all one-particle irreducible diagrams at different orders. For instance, $\mathbf{\Sigma}_R$ has the following perturbative series expansion:

$\Sigma_R =$  (9)

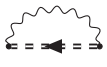
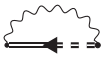
The wiggly lines represent the effective *interaction* and the number of such lines is a measure of the order in the perturbation series. The series representation for Σ_A can be obtained by replacing the solid straight lines with dashed lines. On the other hand, the Keldysh component Σ_K has, in principle, more terms at each order depending on the position of the Keldysh component g_K.

$\Sigma_K =$  (10)

Incidentally, the delta correlation of the disorder [Eq. (2)] helps simplify the diagrammatic series for self-energy drastically, since all the diagrams involving a crossing of two wiggly lines vanish [74]. This is a consequence of the causal (anticausal) structure of the retarded (advanced) Green's function. Consequently, the self-energy consists of only the rainbow-type diagrams and can be exactly resummed using the self-consistent Born approximation (SCBA) [74,79], which is exact rather than an approximation in our case. Quantitatively, we can write in frequency space,

$$\mathbf{\Sigma} = \gamma\int\frac{dk}{2\pi}\int\frac{d\omega}{2\pi}\mathbf{G}(k,\omega). \quad (11)$$

In terms of diagrams, this implies

$\Sigma_R =$ , $\Sigma_A =$ , $\Sigma_K =$  (12)

where the double lines indicate the full Green's function. We notice immediately from Eq. (11) that the self-energy is not dependent on ω and k. This is again a signature of uncorrelated stochastic noise in space and time [Eq. (2)]. The retarded and advanced components turn out to have very simple forms $\Sigma_{R(A)} = \mp i\gamma/2$, which is equal to the contribution from the first-order rainbow diagram. In fact, all the higher-order diagrams for Σ_R and Σ_A can be shown to be precisely equal to zero. The Keldysh self-energy, on the contrary, is slightly nontrivial to derive and depends on T and μ of the reservoirs. Assuming $T = 0$ for the reservoirs, we have (detailed calculations of the self-energies provided in Appendix C)

$$\Sigma_K = -\frac{4i\gamma}{\pi}\int_0^{\pi}\frac{dk}{2\pi}\arctan\Big(\frac{\mathcal{E}(k)-\mu}{\Delta+\gamma/2}\Big). \quad (13)$$

The Dyson equation, along with the self-energy expressions, yields exact formulas for the different components of $\mathbf{G}$:

$$G_{R(A)}(k,\omega) = \frac{1}{\omega-\mathcal{E}(k)\pm i(\Delta+\gamma/2)},$$
$$G_K(k,\omega) = \lim_{T\to 0}\frac{\Sigma_K - 2i\Delta\tanh\left(\frac{\omega-\mu}{2T}\right)}{[\omega-\mathcal{E}(k)]^2+(\Delta+\gamma/2)^2}. \quad (14)$$

V. STEADY-STATE PERSISTENT CURRENT

We now use these steady-state Green's functions to evaluate the persistent current. Of particular interest is G_K, which determines (details provided in Appendix D) the nonequilibrium steady-state occupation function $n(k) = \frac{1}{2}[1 - i\int\frac{d\omega}{2\pi}G_K(k,\omega)]$.

Instead of a discrete sum over the energy levels, we express PC as a Fourier series in flux (details of the calculations to be found in Appendix E) exploiting the flux periodicity:

$$I(\phi) = -\frac{e}{2\pi}\sum_{m=-\infty}^{\infty}e^{i2\pi m\frac{\phi}{\phi_0}}\int_{-\pi}^{\pi}dk\; v(k)n(k)e^{-i(mL)k}, \quad (15)$$

where $v(k) = \partial\mathcal{E}(k)/\partial k$ is the electron velocity at k. Thus, the computation of PC requires the knowledge of the nonequilibrium distribution function. Evaluating Eq. (15) using $n(k)$ from Eq. (14), we obtain the behavior of PC for different values of the noise strength γ and bath hybridization Δ. In Fig. 1(b), we plot the PC (in units of $I_0 = ev_F/L$) as a function of flux ϕ/ϕ_0 for three sets of parameter values $(\gamma,\Delta) = (0, 0.1)$, $(10^{-3}, 10^{-2})$, and $(10^{-2}, 10^{-3})$, which shows typical oscillatory behavior with different amplitudes. We note that

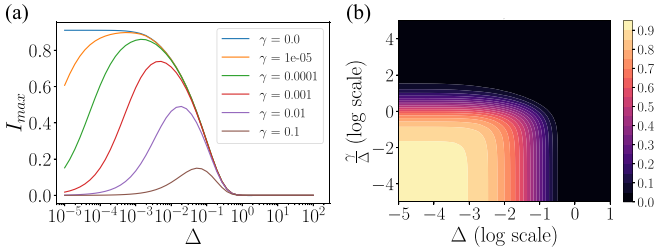


FIG. 2. (a) Amplitude of the persistent current ($I_{\max}$) plotted as a function of the bath hybridization function Δ, for different values of the noise strength γ. For nonzero γ, $I_{\max}$ exhibits nonmonotonic behavior showing first a growth, then a peak, and finally decay with increasing Δ. We fix $L = 16$ and $N = 8$, respectively. (b) Two independent and distinct mechanisms for the suppression of the persistent current are revealed, if $I_{\max}$ is plotted as a function of the pair of parameters $(\gamma/\Delta, \Delta)$, as opposed to (γ, Δ).

throughout the text, the numerical values of these parameters are taken to be in the units of t, the hopping parameter.

We now look at the variation of the amplitude of the PC ($I_{\max}$) at $T = 0$, as a function of Δ and γ. Surprisingly, instead of an overall suppression from the additive effects of noise and the fermionic reservoir, they compete, leading to an unusual nonmonotonic current. In Fig. 2(a), we show $I_{\max}$ as a function of Δ in a semi-log plot for different noise strengths $\gamma = 0, 10^{-5}, \ldots, 10^{-1}$. Here, I_0 is the current carried by an electron at the Fermi level, with v_F being the Fermi velocity of the electrons in the ring. The system size is $L = 16$ with $N = 8$ fermions.

We observe in Fig. 2(a) that for nonzero γ, $I_{\max}$ first increases with increasing Δ, reaches a maximum, and then decays to zero. We also notice that the position of the peak of $I_{\max}$ shifts toward smaller Δ as γ gets smaller and the maximum becomes flatter or plateaulike. Additionally, for $\gamma = 0$, $I_{\max}$ shows monotonic behavior without any maximum at any Δ. Furthermore, the decay at large Δ is seen to be almost independent of the value of γ. This suggests the existence of a sweet spot in the parameter space, where the PC is not appreciably affected. Nevertheless, two distinct pathways exist that destroy phase coherence in the system and suppress the PC.

VI. TWO MECHANISMS OF DECOHERENCE

The two independent routes for suppression of the PC become more apparent, once we look at the contour plot of $I_{\max}$ as a function of Δ and γ/Δ, instead of γ and Δ, as shown in Fig. 2(b). It clearly suggests that for a fixed Δ, the ratio of noise to reservoir coupling γ/Δ provides an independent channel of decoherence and vice versa. In the absence of the reservoirs ($\Delta = 0$), the presence of noise ($\gamma \neq 0$) will heat the system up to an infinite-temperature steady state. We now turn to inspect each of these two mechanisms, driven by Δ and γ/Δ, respectively, more closely.

A. Reservoir-induced decoherence

In Fig. 3(a), we look at the behavior of $I_{\max}$ as a function of Δ for different system sizes $L = 8, 16, \ldots, 120$ at half

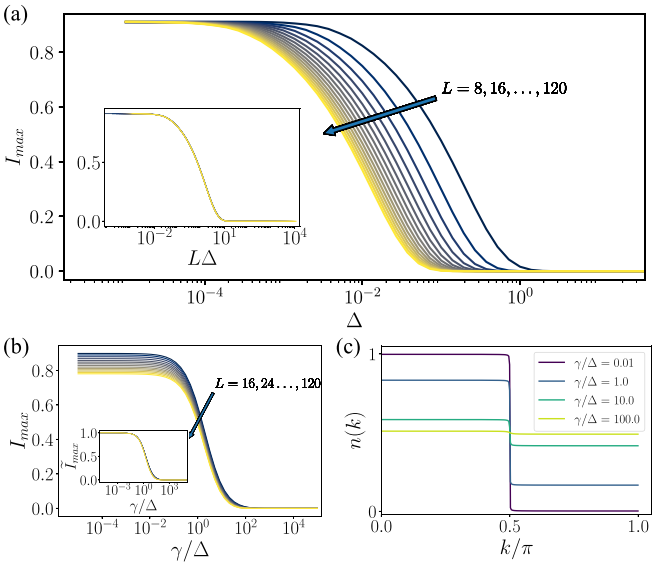


FIG. 3. (a) Plot for $I_{\max}$ as a function of Δ for different system sizes $L = 8, 16, \ldots, 120$ at half filling in the absence of noise ($\gamma = 0$). The curves show a systematic L dependence and excellent scaling collapse if plotted as a function of $L\Delta$ [inset of panel (a)], leading to the notion of a coherence length scale $\xi_\Delta = v_F/\Delta$. (b) $I_{\max}$ as a function of the ratio γ/Δ for different $L = 16, 24, \ldots, 120$ at half filling for fixed $\Delta = 0.001$. Except for the peak values, the curves are almost independent of L, which becomes clear if each of the curves is normalized by its peak value and plotted for different L [inset of panel (b)]. (c) The momentum occupation function $n(k)$ for different ratios $\gamma/\Delta = 0.01, 1, \ldots 100$ at a given $\Delta = 0.001$. As γ/Δ increases, $n(k)$ becomes progressively flatter, though the sharp jump at $k_F = \pi/2$ persists indicating the emergence of a pure nonequilibrium state distinct from a high-temperature equilibrium state.

filling, in the absence of noise γ or equivalently the ratio $\gamma/\Delta = 0$. We immediately see that $I_{\max}$ shows a systematic system-size dependence, and the curves show a reasonably good scaling collapse once we rescale Δ by the system size L [inset of Fig. 3(a)]. We infer that for a fixed γ/Δ, the decay of maximum persistent current follows a universal function $I_{\max}/I_0 \sim \mathscr{I}(L\Delta)$, with $I_{\max}$ dropping to zero once $L\Delta$ exceeds 1. This prompts us to define a coherence length scale $\xi_\Delta \sim 1/\Delta$ (modulo a factor of Fermi velocity $v_F \approx 2t$) induced by the reservoirs, beyond which the phase coherence of the system is lost and PC is suppressed. Equivalently, in terms of energy scales, reservoir-induced decoherence becomes significant when Δ exceeds characteristic level spacing $\delta E = t/L$.

B. Decoherence driven by noise to reservoir ratio

In the regime of small reservoir coupling, the decoherence is driven by the ratio of noise to reservoir coupling γ/Δ. The variation of $I_{\max}$ as a function of γ/Δ, for fixed $\Delta = 10^{-3}$, shows little to no dependence on the system size L, except for the peak values, as shown in Fig. 3(b). Accordingly, the normalized $\widetilde{I}_{\max}$, obtained by dividing each of the curves by the respective peak values, can be seen to be almost independent of L as shown in the inset of Fig. 3(b). Hence,

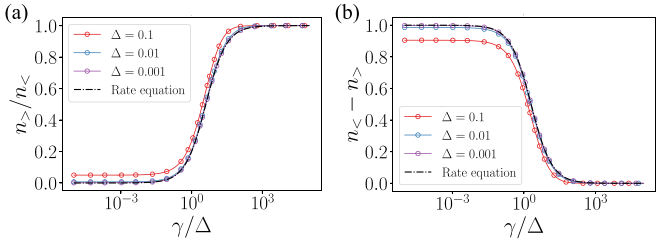


FIG. 4. (a) Ratio of steady-state average occupation above ($n_>$) and below ($n_<$) the Fermi energy obtained using Keldysh calculation for different $\Delta = 0.1, 0.01,$ and 0.001 contrasted with the same obtained from the classical rate equations (16). (b) The difference of steady-state average occupation $n_< - n_>$ for the same values of Δ as panel (a) contrasted with rate equation calculations.

this mechanism of decoherence cannot be associated with a length scale. However, the steady-state occupation function $n(k)$ for different values of the ratio γ/Δ for given $\Delta = 10^{-3}$ exhibits interesting behavior. We notice in Fig. 3(c) that as the ratio of noise to reservoir coupling γ/Δ increases, states at $k > k_F = \pi/2$ start filling up, while states at $k \leqslant k_F$ start getting depleted. This causes $n(k)$ to become flatter, although the discontinuous jump at the Fermi momentum k_F remains. A flatter distribution implies that occupation probabilities are similar for states close in energy, carrying currents of either sign. The positive and negative contributions to the current cancel each other out significantly, leading to the suppression of the PC. In contrast, the distribution function of a higher-temperature equilibrium state is rounded with a broadening of the edge at k_F.

Empirically, this steady state can be understood using classical rate equations for momentum occupations. Spatially uncorrelated noise scatters fermions between filled and empty states regardless of momentum. As a result, the momentum distribution tends to be flatter. The retarded and advanced self-energies indicate that the scattering rate or strength is $\gamma/2$. Conversely, the reservoir will tend to relax the occupation of each momentum state toward the Fermi-Dirac distribution (at $T = 0$) of the bath. Defining the average occupation above and below Fermi energy μ as $n_{>(<)} = \frac{2}{L}\sum_{|k|>(\leqslant)k_F} n_k$, with the constraint $n_> + n_< = 1$, we finally arrive at

$$\frac{dn_<}{dt} = -\frac{\gamma}{4}(n_< - n_>) - \Delta(n_< - 1),$$
$$\frac{dn_>}{dt} = -\frac{\gamma}{4}(n_> - n_<) - \Delta n_>. \tag{16}$$

In the steady state, the derivatives are zero as there is no transfer of particles. The average steady-state population is then given by

$$n_< = \frac{4\Delta + \gamma}{2(2\Delta + \gamma)}, \quad n_> = 1 - n_<. \tag{17}$$

In Fig. 4, we contrast the ratio of occupations $n_>/n_<$ [panel (a)] and the difference of occupations $n_>$ and $n_<$ [panel (b)], obtained from rate equation calculations to those from Keldysh calculations for varied $\Delta = 0.1, 0.01,$ and 0.001. The two approaches show remarkable agreement with decreasing Δ, suggesting that the classical rate equation can efficiently describe the emergent steady state due to the interplay of noise and reservoir.

VII. CONCLUSION AND PERSPECTIVES

To summarize, the nonmonotonic behavior in the PC arises due to the competition between the stochastic noise and reservoir. In particular, the origin of the two mechanisms can be understood from the distinct effects of the reservoir couplings. For weak reservoir coupling, the reservoirs essentially help maintain the Fermi-Dirac distribution of the ring electrons counteracting the noise that tends to flatten the distribution. Increasing Δ for a fixed noise γ therefore initially enhances the current. At stronger coupling, however, the reservoirs broaden the energy levels and introduce a finite coherence length set by $\xi_\Delta = v_F/\Delta$. Once Δ becomes comparable to the characteristic level spacing δE ($\sim t/L$), or equivalently, the coherence length scale becomes equivalent to or shorter than the system size $\xi_\Delta \lesssim L$, reservoir-induced decoherence takes over. Therefore, increasing Δ further supresses the persistent current irrespective of γ. Thus, the two regimes are controlled by the competing scales γ/Δ and $\Delta/\delta E$, respectively, with the persistent current saturating in the window $\gamma \lesssim \Delta \lesssim \delta E$.

A natural extension is to incorporate interactions in the nonequilibrium scenario, as in equilibrium, attractive interactions can enhance the current while repulsive interaction typically suppresses it [27,34,38]. Another interesting direction would be to study the time evolution of the system toward this nonequilibrium steady state. Moreover, we believe our results could be accessible in ultracold-atom experiments, where realization of persistent currents in fermionic rings [51,52,97], fermionic reservoirs [98,99], and external noise [100,101] has already been possible.

ACKNOWLEDGMENTS

We thank Christophe Berthod for illuminating discussions and comments on the manuscript. We also acknowledge Géraldine Haack, Diptiman Sen, and Catalin-Mihai Halati for useful discussions and suggestions. This work was supported by the Swiss National Science Foundation under Division II (Grant No. 200020-219400).

DATA AVAILABILITY

There are no publicly available research data or software supporting this manuscript. Requests for further information or data should be sent to the authors.

APPENDIX A: DERIVATION OF EFFECTIVE ACTION BY INTEGRATING OUT THE RESERVOIR FERMIONS

We present here the details of the derivation of the effective action by integrating the reservoir fermions. The Keldysh partition function of the system-reservoir composite is given as

$$Z = \int \mathcal{D}(\bar{\psi}, \psi) \int \mathcal{D}(\bar{c}, c) e^{i[S_s(\bar{\psi},\psi) + S_b(\bar{c},c) + Ss - b(\bar{\psi},\psi,\bar{c},c)]}, \tag{A1}$$

where the partition function involving the bath and the system-bath coupling in Fourier space is given by

$$\begin{aligned} Z_{\text{bath}} &= \int \mathcal{D}(\bar{c},c)e^{i(S_b+S_{s-b})} \\ &= \int \mathcal{D}(\bar{c},c)\exp\Bigg[i\sum_{j=1}^{L}\int\frac{dq}{2\pi}\int\frac{d\omega}{2\pi} \\ &\quad\times \begin{pmatrix}\bar{c}_j^1(q,\omega) & \bar{c}_j^2(q,\omega)\end{pmatrix} \\ &\quad\times \begin{pmatrix}\omega-E_q+i\eta & 2i\eta\tanh\left(\frac{\omega-\mu}{2T}\right)\\ 0 & \omega-E_q-i\eta\end{pmatrix}\begin{pmatrix}c_j^1(q,\omega)\\ c_j^2(q,\omega)\end{pmatrix} \\ &\quad+\tau_c\begin{pmatrix}\bar{c}_j^1(q,\omega) & \bar{c}_j^2(q,\omega)\end{pmatrix}\begin{pmatrix}\psi_j^1(\omega)\\ \psi_j^2(\omega)\end{pmatrix} \\ &\quad+\tau_c\begin{pmatrix}\bar{\psi}_j^1(\omega) & \bar{\psi}_j^2(\omega)\end{pmatrix}\begin{pmatrix}c_j^1(q,\omega)\\ c_j^2(q,\omega)\end{pmatrix}\Bigg]. \end{aligned} \tag{A2}$$

We evaluate this Gaussian integral on the $(\bar{c},c)$ Grassmann fields using the Hubbard–Stratonovich transformation to obtain

$$\begin{aligned} Z_{\text{bath}} = \int \mathcal{D}(\bar{c},c)\exp\Bigg[&-i\tau_c^2\int\frac{d\omega}{2\pi}\sum_{j=1}^{L}\begin{pmatrix}\bar{\psi}_j^1(\omega) & \bar{\psi}_j^2(\omega)\end{pmatrix} \\ &\times\int\frac{dq}{2\pi}\begin{pmatrix}G^R_{\text{bath}}(q,\omega) & G^K_{\text{bath}}(q,\omega)\\ 0 & G^A_{\text{bath}}(q,\omega)\end{pmatrix}\begin{pmatrix}\psi_j^1(\omega)\\ \psi_j^2(\omega)\end{pmatrix}\Bigg]. \end{aligned} \tag{A3}$$

We introduce the reservoir Green's functions $G^{R(A)}_{\text{bath}}(q,\omega)=\frac{1}{\omega-(E_q-\mu)\pm i\eta}$ and $G^K_{\text{bath}}(q,\omega)=-2\pi i\tanh(\frac{\omega-\mu}{2T})\delta(\omega-E_q)$. Momentum integration on these Green's functions requires the knowledge of the reservoir dispersion E_q. We assume the reservoir dispersion to be linear with a corresponding Fermi momentum (velocity) given by $q_F(\mathbb{v}_F)$. The chemical potential is therefore given by $\mu=q_F$, since we have set $\hbar=1$. Consequently, the dispersion is given as

$$E_q=\begin{cases}\mathbb{v}_F(q-q_F), & |q-q_F|\leqslant\Lambda,\\ -\mathbb{v}_F(q+q_F), & |q+q_F|\leqslant\Lambda,\end{cases} \tag{A4}$$

where we have put a large cutoff Λ in momentum for regularization. The integrals can now be performed with this dispersion,

$$\begin{aligned} \int\frac{dq}{2\pi}G^{R(A)}_{\text{bath}}(q,\omega) &= \int\frac{dq}{2\pi}\frac{1}{\omega-(E_q-\mu)\pm i\eta} \\ &= \int_{-\Lambda}^{\Lambda}\frac{dq}{2\pi}\frac{1}{\omega-\mathbb{v}_F q\pm i\eta} \\ &\quad+\int_{-\Lambda}^{\Lambda}\frac{dq}{2\pi}\frac{1}{\omega+\mathbb{v}_F q\pm i\eta}. \end{aligned} \tag{A5}$$

Next, we take the limit $\Lambda\to\infty$ and use the Sokhotski-Plemelj theorem, which states $\frac{1}{x+i\eta}=\text{P.V.}(\frac{1}{x})\mp i\pi\delta(x)$ as $\eta\to 0$. Here, P.V. denotes the Cauchy principle value. This yields finally

$$\int\frac{dq}{2\pi}G^{R(A)}_{\text{bath}}(q,\omega)=\mp\frac{1}{\mathbb{v}_F}. \tag{A6}$$

On the contrary, the Dirac delta function in $G^K_{\text{bath}}(q,\omega)$ can be easily integrated due to the linearity of dispersion

$$\int\frac{dq}{2\pi}G^K_{\text{bath}}(q,\omega)=-\frac{2i}{\mathbb{v}_F}\tanh\left(\frac{\omega-\mu}{2T}\right). \tag{A7}$$

The entire partition function can therefore be rewritten as $Z=\int\mathcal{D}(\bar{\psi},\psi)e^{i(S_s+S')}$, where S' is the resulting action after integrating the reservoir fermions and has the following expression:

$$\begin{aligned} S' = i\frac{\tau_c^2}{\mathbb{v}_F}\sum_{j=1}^{L}\int\frac{d\omega}{2\pi}&\begin{pmatrix}\bar{\psi}_j^1(\omega) & \bar{\psi}_j^2(\omega)\end{pmatrix} \\ &\times\begin{pmatrix}1 & 2\tanh\left(\frac{\omega-\mu}{2T}\right)\\ 0 & 1\end{pmatrix}\begin{pmatrix}\psi_j^1(\omega)\\ \psi_j^2(\omega)\end{pmatrix}. \end{aligned} \tag{A8}$$

Subsequently, we introduce bath hybridization function $\Delta=\frac{\tau_c^2}{\mathbb{v}_F}$ and perform a Fourier transform of the fermionic fields as $\psi_j=\frac{1}{L}\sum_k\psi_k e^{-ikj}$, while the inverse Fourier transform is $\psi_k=\sum_{j=1}^{L}\psi_j e^{ikj}$. The Fourier transform of the $\bar{\psi}$ fields can be done by conjugation to ensure anticommutation relations in momentum space as well. Finally, taking the continuum limit in the discrete momentum sum $\sum_k\to L\int dk/2\pi$ yields Eq. (4).

APPENDIX B: AVERAGING THE STOCHASTIC DISORDER: EFFECTIVE QUARTIC INTERACTION

The Keldysh action involving the stochastic disorder is

$$\begin{aligned} S_{\text{dis}} &= -\sum_j\int_{\mathcal{C}}dtV_j(t)\bar{\psi}_j(t)\psi_j(t) \\ &= -\sum_j\int_{-\infty}^{\infty}dtV_j(t)\left[\bar{\psi}_j^1(t)\psi_j^1(t)+\bar{\psi}_j^2(t)\psi_j^2(t)\right] \\ &= -\sum_j\int_{-\infty}^{\infty}dtV_j(t)\rho_j(t), \end{aligned} \tag{B1}$$

where $\mathcal{C}$ under the time integral denotes the Keldysh contour, the second equality is coming due to the LO rotation of the fields in the Keldysh space [95], and $\rho_j(t)=[\bar{\psi}_j^1(t)\psi_j^1(t)+\bar{\psi}_j^2(t)\psi_j^2(t)]$. The disorder $V_j(t)$ is a white noise that follows the Gaussian distribution

$$P[V]=\exp\left(-\frac{1}{2}\sum_{i,j}\int_{-\infty}^{\infty}dt\int_{-\infty}^{\infty}dt'V_i(t)D_{ij}^{-1}(t-t')V_j(t)\right), \tag{B2}$$

with the variance of the distribution being $\overline{V_i(t)V_j(t')}=D_{ij}(t-t')=2\gamma\delta_{ij}\delta(t-t')$. Since in Keldysh formalism the observables are obtained from the Keldysh partition function as opposed to the logarithm of it, as in equilibrium formalism, the disorder averaging is performed over Z. If S_0 represents

the action for the nondisordered part of system, the disorder averaging proceeds as follows:

$$\begin{aligned}\overline{Z} &= \int \mathcal{D}(\bar{\psi},\psi)e^{iS_0}\int \mathcal{D}V\,P[V]e^{iS_{dis}[V]}\\ &= \int \mathcal{D}(\bar{\psi},\psi)e^{iS_0}\int \mathcal{D}V\,\exp\Bigg[-i\sum_j\int_{-\infty}^{\infty}dtV_j(t)\rho_j(t)\\ &\quad -\frac{1}{2}\sum_{j,l}\int_{-\infty}^{\infty}dt'V_j(t)D_{jl}^{-1}(t-t')V_l(t)\Bigg]. \end{aligned} \tag{B3}$$

In the above expression, $\int \mathcal{D}V$ can be evaluated exactly, since it is a Gaussian integral, leading to an expression that is quadratic in ρ. This yields

$$\begin{aligned}\overline{Z} &= \int \mathcal{D}(\bar{\psi},\psi)e^{iS_0}\exp\Bigg[\frac{(-i)^2}{2}\sum_{l,j}\int_{-\infty}^{\infty}dt\\ &\quad\times\int_{-\infty}^{\infty}dt'\rho_j(t)D_{jl}(t-t')\rho_l(t')\Bigg]\\ &= \int \mathcal{D}(\bar{\psi},\psi)e^{iS_0}\exp\Bigg[-\gamma\sum_j\int_{-\infty}^{\infty}dt\,\rho_j(t)\rho_j(t)\Bigg]\\ &= \int \mathcal{D}(\bar{\psi},\psi)e^{iS_0}\\ &\quad\times\exp\Bigg[-\gamma\sum_j\int_{-\infty}^{\infty}\left(\bar{\psi}_j^1(t)\psi_j^1(t)+\bar{\psi}_j^2(t)\psi_j^2(t)\right)\\ &\quad\times\left(\bar{\psi}_j^1(t)\psi_j^1(t)+\bar{\psi}_j^2(t)\psi_j^2(t)\right)dt\Bigg]. \end{aligned} \tag{B4}$$

We have used the delta function correlation of the disorder $D_{jl}(t-t')$. Finally, Fourier transforming the fields we arrive at the effective action involving quartic interaction mentioned in the main text.

APPENDIX C: SCBA SELF-ENERGY

We start with the bare Green's functions given in Eq. (5), which denotes the nondisordered part of the action. As explained in the main text, SCBA provides an exact method to obtain the self-energy in our case due to the delta correlation of the disorder (also see Refs. [74,79]). The equation for SCBA self-energy is $\mathbf{\Sigma} = \gamma\int\frac{dk}{2\pi}\int\frac{d\omega}{2\pi}\mathbf{G}(k,\omega)$, which for retarded and advanced components becomes

$$\Sigma_{R(A)} = \gamma\int_{-\pi}^{\pi}\frac{dk}{2\pi}\int_{-\infty}^{\infty}\frac{d\omega}{2\pi}\frac{1}{\omega-\mathcal{E}(k)\pm i\Delta-\Sigma_{R(A)}}. \tag{C1}$$

The limits of the ω integral being $-\infty$ to ∞, the integral is fairly straightforward and is given by $\Sigma^{R(A)} = \mp\frac{i}{2}\gamma$. The full retarded and advanced Green's functions become

$$\begin{aligned}G_R(k,\omega) &= \frac{1}{\omega-\mathcal{E}(k)+i(\Delta+\gamma/2)},\\ G_A(k,\omega) &= \frac{1}{\omega-\mathcal{E}(k)-i(\Delta+\gamma/2)}. \end{aligned} \tag{C2}$$

The Keldysh self-energy is slightly tricky to obtain. The SCBA equation for the Keldysh component of the self-energy reads

$$\begin{aligned}\Sigma_K &= \gamma\int_{-\pi}^{\pi}\frac{dp_1}{2\pi}\int_{-\infty}^{\infty}\frac{d\omega_1}{2\pi}G_K(p_1,\omega_1)\\ &= -\gamma\int_{-\pi}^{\pi}\frac{dp_1}{2\pi}\int_{-\infty}^{\infty}\frac{d\omega_1}{2\pi}[G_R([g^{-1}]_K-\Sigma_K)G_A]\\ &= \gamma\int_{-\pi}^{\pi}\frac{dp_1}{2\pi}\int_{-\infty}^{\infty}\frac{d\omega_1}{2\pi}G_R(p_1,\omega_1)\Sigma_K G_A(p_1,\omega_1)\\ &\quad-\gamma\int_{-\pi}^{\pi}\frac{dp_1}{2\pi}\int_{-\infty}^{\infty}\frac{d\omega_1}{2\pi}\frac{2i\Delta\tanh\left(\frac{\omega_1-\mu}{2T}\right)}{(\omega_1-\mathcal{E}(p_1))^2+(\Delta+\gamma/2)^2}. \end{aligned} \tag{C3}$$

Next, we take the limit of $T\to 0$, causing the tanh function to approach a step function asymptotically and therefore the integral in the second term becomes tractable. We also take the first term to the left-hand side of the equation and arrive at

$$\begin{aligned}&\Sigma_K\left(1-\gamma\int_{-\pi}^{\pi}\frac{dp_1}{2\pi}\int_{-\infty}^{\infty}\frac{d\omega_1}{2\pi}\frac{1}{(\omega_1-\mathcal{E}(p_1))^2+(\Delta+\gamma/2)^2}\right)\\ &= -2i\Delta\gamma\int_{-\pi}^{\pi}\frac{dp_1}{2\pi}\frac{2}{2\pi(\Delta+\gamma/2)}\arctan\left(\frac{\mathcal{E}(p_1)-\mu}{\Delta+\gamma/2}\right),\\ &\Rightarrow\Sigma_K\left(1-\frac{\gamma}{2(\Delta+\gamma/2)}\right)\\ &= -\frac{2i\Delta\gamma}{\pi(\Delta+\gamma/2)}\int_{-\pi}^{\pi}\frac{dp_1}{2\pi}\arctan\left(\frac{\mathcal{E}(p_1)-\mu}{\Delta+\gamma/2}\right). \end{aligned} \tag{C4}$$

After final rearrangements, this yields the expression for the Keldysh self-energy at $T=0$ given in Eq. (10):

$$\Sigma_K = -\frac{4i\gamma}{\pi}\int_0^{\pi}\frac{dk}{2\pi}\arctan\left(\frac{\mathcal{E}(k)-\mu}{\Delta+\gamma/2}\right). \tag{C5}$$

It should be noted that the self-energies are constant and not functions of p and ω, due to the delta function correlation of the stochastic noise.

APPENDIX D: NONEQUILIBRIUM OCCUPATION FUNCTION FROM THE KELDYSH GREEN'S FUNCTION

In a nonequilibrium steady state, i.e., when the correlation functions of the system only depend on the relative time, the Keldysh Green's function is related to the retarded and

advanced Green's function as

$$G^K(k,\omega) = F(\omega)[G^R(k,\omega) - G^A(k,\omega)] = (1-2f(\omega))[G^R(k,\omega) - G^A(k,\omega)], \quad \text{(D1)}$$

where $f(\omega)$ is the nonequilibrium distribution function. The spectral function $A(\omega)$ is also related to the retarded and advanced Green's function as

$$A(k,\omega) = i[G^R(k,\omega) - G^A(k,\omega)]. \quad \text{(D2)}$$

In addition, the spectral function also obeys the following sum rules:

$$\int \frac{d\omega}{2\pi} A(k,\omega) = 1, \quad \int \frac{d\omega}{2\pi} f(\omega) A(k,\omega) = n(k). \quad \text{(D3)}$$

The second equation in Eq. (D3) and Eq. (D2) trivially lead to the relation between $G^K(k,\omega)$ and $n(k)$:

$$n(k) = \frac{1}{2}\left[1 - i\int_{-\infty}^{\infty} d\omega/2\pi G^K(k,\omega)\right]. \quad \text{(D4)}$$

APPENDIX E: EXPRESSION FOR THE PERSISTENT CURRENT AS A FOURIER SERIES IN MAGNETIC FLUX

In this Appendix, we will derive the general expression for the persistent current, presented in Eq. (12). This expresses the persistent current as a Fourier series in the magnetic flux and the Fourier coefficients contain the occupation distribution, which can account for both equilibrium or nonequilibrium cases. Our starting point is the discrete sum in Eq. (3):

$$I = -\frac{e}{L}\sum_n v_n(\phi) f(\mathcal{E}_n(\phi)). \quad \text{(E1)}$$

Here, $f(\mathcal{E})$ is the distribution function. For a tight-binding ring with L number of sites, the energy levels are $\mathcal{E}_n(\phi) = -2t\cos[\frac{2\pi}{L}(n+\phi/\phi_0)] = \mathcal{E}(n+\phi/\phi_0)$, and subsequently, the velocities of those levels are $v_n(\phi) = 2t\sin[\frac{2\pi}{L}(n+\phi/\phi_0)] = v(n+\phi/\phi_0)$, and n ranges from $-L/2$ to $L/2-1$.

Let us define two functions $\zeta(n+\phi/\phi_0) = v(n+\phi/\phi_0) f(\mathcal{E}(n+\phi/\phi_0))$ and $\xi(\phi/\phi_0) = \sum_{n=-L/2}^{L/2-1}\zeta(n+\phi/\phi_0)$. Then,

$$\xi(\phi/\phi_0+1) = \sum_{n=-L/2}^{L/2-1}\zeta(n+1+\phi/\phi_0) = \sum_{n=-L/2+1}^{L/2}\zeta(n+\phi/\phi_0) = \xi(\phi/\phi_0) + \zeta(L/2+\phi/\phi_0) - \zeta(-L/2+\phi/\phi_0). \quad \text{(E2)}$$

However, $\zeta(L/2+\phi/\phi_0) - \zeta(-L/2+\phi/\phi_0) = 0$, since $v(L/2+\phi/\phi_0) = v(-L/2+\phi/\phi_0)$ and $\mathcal{E}(L/2+\phi/\phi_0) = -\mathcal{E}(-L/2+\phi/\phi_0)$. These relations along with Eq. (E2) lead to the fact that

$$\xi(\phi/\phi_0+1) = \xi(\phi/\phi_0), \quad \text{(E3)}$$

or in other words $\xi(\phi/\phi_0)$ is a periodic function with period 1. This suggests that $\xi(\phi/\phi_0)$ admits a Fourier series in ϕ/ϕ_0:

$$\xi(\phi/\phi_0) = \sum_{m=-\infty}^{\infty}\widetilde{\xi}(m)e^{i2\pi m\phi/\phi_0}, \quad \widetilde{\xi}(m) = \int_0^1 dy\,\xi(y)e^{-i2\pi my}. \quad \text{(E4)}$$

Thus, using the relation between ζ and ξ, we can write

$$\widetilde{\xi}(m) = \int_0^1 dy\sum_{n=-L/2}^{L/2}\zeta(n+y)e^{-i2\pi my} = \int_{-L/2}^{L/2} dy\,\zeta(y)e^{-i2\pi my} = \int_{-\pi}^{\pi}\frac{L}{2\pi}dk\,\zeta\left(\frac{Lk}{2\pi}\right)e^{-imLk}, \quad \text{(E5)}$$

where we have defined a new variable $k = \frac{2\pi y}{L}$. This redefinition helps simplifying the expression as $\zeta(\frac{Lk}{2\pi}) = v(k)f(\mathcal{E}(k))$, with $\mathcal{E}(k) = -2t\cos(k)$ and $v(k) = 2t\sin(k)$. We can now simply replace $f(\mathcal{E}(k))$ with $n(k)$, the momentum space occupation function.

The expression for persistent current can now be expressed as

$$I = -\frac{e}{L}\sum_n v_n(\phi)f(\mathcal{E}_n(\phi)) = -\frac{e}{L}\xi(\phi/\phi_0) = -\frac{e}{L}\sum_{m=-\infty}^{\infty}\left\{\frac{L}{2\pi}\int_{-\pi}^{\pi}dk\,v(k)n(k)e^{-imLk}\right\}e^{i2\pi m\phi/\phi_0} = -\frac{e}{2\pi}\sum_{m=-\infty}^{\infty}e^{i2\pi m\frac{\phi}{\phi_0}}\int_{-\pi}^{\pi}dk\,v(k)n(k)e^{-i(mL)k}. \quad \text{(E6)}$$

This is precisely the expression for persistent current given in Eq. (12).

[1] R. Feynman and F. Vernon, The theory of a general quantum system interacting with a linear dissipative system, Ann. Phys. (NY) **281**, 547 (2000).

[2] A. Caldeira and A. Leggett, Path integral approach to quantum Brownian motion, Phys. A: Stat. Mech. Appl. **121**, 587 (1983).

[3] C. W. Gardiner and P. Zoller, *Quantum Noise: A Handbook of Markovian and Non-Markovian Quantum Stochastic Methods with Applications to Quantum Optics* (Springer Berlin, Heidelberg, 2004).

[4] A. A. Clerk, M. H. Devoret, S. M. Girvin, F. Marquardt, and R. J. Schoelkopf, Introduction to quantum noise, measurement, and amplification, Rev. Mod. Phys. **82**, 1155 (2010).

[5] M. V. Medvedyeva, F. H. L. Essler, and T. Prosen, Exact Bethe ansatz spectrum of a tight-binding chain with dephasing noise, Phys. Rev. Lett. **117**, 137202 (2016).

[6] A. Bastianello, J. De Nardis, and A. De Luca, Generalized hydrodynamics with dephasing noise, Phys. Rev. B **102**, 161110(R) (2020).

[7] B. Skinner, J. Ruhman, and A. Nahum, Measurement-induced phase transitions in the dynamics of entanglement, Phys. Rev. X **9**, 031009 (2019).

[8] O. Alberton, M. Buchhold, and S. Diehl, Entanglement transition in a monitored free-fermion chain: From extended criticality to area law, Phys. Rev. Lett. **126**, 170602 (2021).

[9] H. M. Wiseman and G. J. Milburn, *Quantum Measurement and Control* (Cambridge University Press, Cambridge, 2009).

[10] S. A. Gurvitz, Measurements with a noninvasive detector and dephasing mechanism, Phys. Rev. B **56**, 15215 (1997).

[11] S. A. Gurvitz, L. Fedichkin, D. Mozyrsky, and G. P. Berman, Relaxation and the Zeno effect in qubit measurements, Phys. Rev. Lett. **91**, 066801 (2003).

[12] C. Carisch, A. Romito, and O. Zilberberg, Quantifying measurement-induced quantum-to-classical crossover using an open-system entanglement measure, Phys. Rev. Res. **5**, L042031 (2023).

[13] M. Buchhold, Y. Minoguchi, A. Altland, and S. Diehl, Effective theory for the measurement-induced phase transition of Dirac fermions, Phys. Rev. X **11**, 041004 (2021).

[14] X. Cao, A. Tilloy, and A. De Luca, Entanglement in a fermion chain under continuous monitoring, SciPost Phys. **7**, 024 (2019).

[15] P. Zhang, C. Liu, S.-K. Jian, and X. Chen, Universal entanglement transitions of free fermions with long-range non-unitary dynamics, Quantum **6**, 723 (2022).

[16] B. Altshuler, M. Gershenson, and I. Aleiner, Phase relaxation of electrons in disordered conductors, Phys. E: Low-Dimens. Syst. Nanostructures **3**, 58 (1998).

[17] I. V. Gornyi, A. D. Mirlin, and D. G. Polyakov, Interacting electrons in disordered wires: Anderson localization and low-T transport, Phys. Rev. Lett. **95**, 206603 (2005).

[18] D. M. Basko, I. L. Aleiner, and B. L. Altshuler, Metal–insulator transition in a weakly interacting many-electron system with localized single-particle states, Ann. Phys. (NY) **321**, 1126 (2006).

[19] F. Hund, Rechnungen über das magnetische verhalten von kleinen metallstücken bei tiefen temperaturen, Ann. Phys. (NY) **424**, 102 (1938).

[20] M. Büttiker, Y. Imry, and R. Landauer, Josephson behavior in small normal one-dimensional rings, Phys. Lett. A **96**, 365 (1983).

[21] H.-F. Cheung, Y. Gefen, and E. K. Riedel, Isolated rings of mesoscopic dimensions. Quantum coherence and persistent currents, IBM J. Res. Dev. **32**, 359 (1988).

[22] H.-F. Cheung, Y. Gefen, E. K. Riedel, and W.-H. Shih, Persistent currents in small one-dimensional metal rings, Phys. Rev. B **37**, 6050 (1988).

[23] H.-F. Cheung, E. K. Riedel, and Y. Gefen, Persistent currents in mesoscopic rings and cylinders, Phys. Rev. Lett. **62**, 587 (1989).

[24] B. L. Altshuler, Y. Gefen, and Y. Imry, Persistent differences between canonical and grand canonical averages in mesoscopic ensembles: Large paramagnetic orbital susceptibilities, Phys. Rev. Lett. **66**, 88 (1991).

[25] A. Schmid, Persistent currents in mesoscopic rings by suppression of charge fluctuations, Phys. Rev. Lett. **66**, 80 (1991).

[26] F. von Oppen and E. K. Riedel, Average persistent current in a mesoscopic ring, Phys. Rev. Lett. **66**, 84 (1991).

[27] V. Ambegaokar and U. Eckern, Coherence and persistent currents in mesoscopic rings, Phys. Rev. Lett. **65**, 381 (1990).

[28] U. Eckern and A. Schmid, Persistent currents of single mesoscopic rings, Europhys. Lett. **18**, 457 (1992).

[29] N. Yu and M. Fowler, Persistent current of a Hubbard ring threaded with a magnetic flux, Phys. Rev. B **45**, 11795 (1992).

[30] S. Fujimoto and N. Kawakami, Persistent currents in mesoscopic Hubbard rings with spin-orbit interaction, Phys. Rev. B **48**, 17406 (1993).

[31] R. A. Smith and V. Ambegaokar, Systematic calculation of moment of flux-dependent currents in single mesoscopic rings, Europhys. Lett. **20**, 161 (1992).

[32] U. Eckern and P. Schwab, Normal persistent currents, Adv. Phys. **44**, 387 (1995).

[33] P. Kopietz, Universal persistent currents in mesoscopic metal rings due to long-range Coulomb interactions, Phys. Rev. Lett. **70**, 3123 (1993).

[34] T. Giamarchi and B. S. Shastry, Persistent currents in a one-dimensional ring for a disordered Hubbard model, Phys. Rev. B **51**, 10915 (1995).

[35] M. Büttiker, Small normal-metal loop coupled to an electron reservoir, Phys. Rev. B **32**, 1846 (1985).

[36] N. Trivedi and D. A. Browne, Mesoscopic ring in a magnetic field: Reactive and dissipative response, Phys. Rev. B **38**, 9581 (1988).

[37] B. Wunsch and A. Chudnovskiy, Persistent current in a ring coupled to an external fermionic reservoir, Phys. E: Low-Dimens. Syst. Nanostructures **22**, 353 (2004).

[38] A. G. Semenov and A. D. Zaikin, Persistent currents in nanorings and quantum decoherence by Coulomb interaction, Phys. Rev. B **80**, 155312 (2009).

[39] O. I. Pâţu and D. V. Averin, Temperature-dependent periodicity of the persistent current in strongly interacting systems, Phys. Rev. Lett. **128**, 096801 (2022).

[40] H. Bouchiat and G. Montambaux, Persistent currents in mesoscopic rings: Ensemble averages and half-flux-quantum periodicity, J. Phys. **50**, 2695 (1989).

[41] G. Montambaux, H. Bouchiat, D. Sigeti, and R. Friesner, Persistent currents in mesoscopic metallic rings: Ensemble average, Phys. Rev. B **42**, 7647 (1990).

[42] H. Bouchiat, G. Montambaux, and D. Sigeti, Persistent currents in mesoscopic rings, conductance, and boundary conditions, Phys. Rev. B **44**, 1682 (1991).

[43] G. Bouzerar and D. Poilblanc, Persistent currents in multichannel interacting systems, Phys. Rev. B **52**, 10772 (1995).

[44] P. Schmitteckert, R. A. Jalabert, D. Weinmann, and J.-L. Pichard, From the Fermi glass towards the Mott insulator in one dimension: Delocalization and strongly enhanced persistent currents, Phys. Rev. Lett. **81**, 2308 (1998).

[45] L. P. Lévy, G. Dolan, J. Dunsmuir, and H. Bouchiat, Magnetization of mesoscopic copper rings: Evidence for persistent currents, Phys. Rev. Lett. **64**, 2074 (1990).

[46] V. Chandrasekhar, R. A. Webb, M. J. Brady, M. B. Ketchen, W. J. Gallagher, and A. W. Kleinsasser, Magnetic response of a single, isolated gold loop, Phys. Rev. Lett. **67**, 3578 (1991).

[47] E. M. Q. Jariwala, P. Mohanty, M. B. Ketchen, and R. A. Webb, Diamagnetic persistent current in diffusive normal-metal rings, Phys. Rev. Lett. **86**, 1594 (2001).

[48] R. Deblock, R. Bel, B. Reulet, H. Bouchiat, and D. Mailly, Diamagnetic orbital response of mesoscopic silver rings, Phys. Rev. Lett. **89**, 206803 (2002).

[49] H. Bluhm, N. C. Koshnick, J. A. Bert, M. E. Huber, and K. A. Moler, Persistent currents in normal metal rings, Phys. Rev. Lett. **102**, 136802 (2009).

[50] A. C. Bleszynski-Jayich, W. E. Shanks, B. Peaudecerf, E. Ginossar, F. von Oppen, L. I. Glazman, and J. G. E. Harris, Persistent currents in normal metal rings, Science **326**, 272 (2009).

[51] L. Amico, D. Anderson, M. Boshier, J.-P. Brantut, L.-C. Kwek, A. Minguzzi, and W. von Klitzing, *Colloquium*: Atomtronic circuits: From many-body physics to quantum technologies, Rev. Mod. Phys. **94**, 041001 (2022).

[52] J. Polo, W. Chetcuti, T. Haug, A. Minguzzi, K. Wright, and L. Amico, Persistent currents in ultracold gases, Phys. Rep. **1137**, 1 (2025).

[53] G. Barontini, R. Labouvie, F. Stubenrauch, A. Vogler, V. Guarrera, and H. Ott, Controlling the dynamics of an open many-body quantum system with localized dissipation, Phys. Rev. Lett. **110**, 035302 (2013).

[54] H. P. Lüschen, P. Bordia, S. S. Hodgman, M. Schreiber, S. Sarkar, A. J. Daley, M. H. Fischer, E. Altman, I. Bloch, and U. Schneider, Signatures of many-body localization in a controlled open quantum system, Phys. Rev. X **7**, 011034 (2017).

[55] T. Tomita, S. Nakajima, I. Danshita, Y. Takasu, and Y. Takahashi, Observation of the Mott insulator to superfluid crossover of a driven-dissipative Bose-Hubbard system, Sci. Adv. **3**, e1701513 (2017).

[56] M. Fitzpatrick, N. M. Sundaresan, A. C. Y. Li, J. Koch, and A. A. Houck, Observation of a dissipative phase transition in a one-dimensional circuit QED lattice, Phys. Rev. X **7**, 011016 (2017).

[57] R. Ma, B. Saxberg, C. Owens, N. Leung, Y. Lu, J. Simon, and D. I. Schuster, A dissipatively stabilized Mott insulator of photons, Nature (London) **566**, 51 (2019).

[58] K. Yamamoto, M. Nakagawa, N. Tsuji, M. Ueda, and N. Kawakami, Collective excitations and nonequilibrium phase transition in dissipative fermionic superfluids, Phys. Rev. Lett. **127**, 055301 (2021).

[59] N. Dogra, M. Landini, K. Kroeger, L. Hruby, T. Donner, and T. Esslinger, Dissipation-induced structural instability and chiral dynamics in a quantum gas, Science **366**, 1496 (2019).

[60] F. Ferri, R. Rosa-Medina, F. Finger, N. Dogra, M. Soriente, O. Zilberberg, T. Donner, and T. Esslinger, Emerging dissipative phases in a superradiant quantum gas with tunable decay, Phys. Rev. X **11**, 041046 (2021).

[61] N. Syassen, D. M. Bauer, M. Lettner, T. Volz, D. Dietze, J. J. Garciá-Ripoll, J. I. Cirac, G. Rempe, and S. Dürr, Strong dissipation inhibits losses and induces correlations in cold molecular gases, Science **320**, 1329 (2008).

[62] K. Sponselee, L. Freystatzky, B. Abeln, M. Diem, B. Hundt, A. Kochanke, T. Ponath, B. Santra, L. Mathey, K. Sengstock, and C. Becker, Dynamics of ultracold quantum gases in the dissipative Fermi-Hubbard model, Quantum Sci. Technol. **4**, 014002 (2019).

[63] M. B. Plenio and S. F. Huelga, Dephasing assisted transport: Quantum networks and biomolecules, New J. Phys. **10**, 113019 (2008).

[64] P. Rebentrost, M. Mohseni, I. Kassal, S. Lloyd, and A. Aspuru-Guzik, Environment-assisted quantum transport, New J. Phys. **11**, 033003 (2009).

[65] S. Viciani, M. Lima, M. Bellini, and F. Caruso, Observation of noise-assisted transport in an all-optical cavity-based network, Phys. Rev. Lett. **115**, 083601 (2015).

[66] C. Maier, T. Brydges, P. Jurcevic, N. Trautmann, C. Hempel, B. P. Lanyon, P. Hauke, R. Blatt, and C. F. Roos, Environment-assisted quantum transport in a 10-qubit network, Phys. Rev. Lett. **122**, 050501 (2019).

[67] L. Corman, P. Fabritius, S. Häusler, J. Mohan, L. H. Dogra, D. Husmann, M. Lebrat, and T. Esslinger, Quantized conductance through a dissipative atomic point contact, Phys. Rev. A **100**, 053605 (2019).

[68] P. Bredol, H. Boschker, D. Braak, and J. Mannhart, Decoherence effects break reciprocity in matter transport, Phys. Rev. B **104**, 115413 (2021).

[69] M.-Z. Huang, J. Mohan, A.-M. Visuri, P. Fabritius, M. Talebi, S. Wili, S. Uchino, T. Giamarchi, and T. Esslinger, Superfluid signatures in a dissipative quantum point contact, Phys. Rev. Lett. **130**, 200404 (2023).

[70] A.-M. Visuri, T. Giamarchi, and C. Kollath, Symmetry-protected transport through a lattice with a local particle loss, Phys. Rev. Lett. **129**, 056802 (2022).

[71] O. Entin-Wohlman, Y. Imry, and A. Aharony, Effects of external radiation on biased Aharonov-Bohm rings, Phys. Rev. B **70**, 075301 (2004).

[72] K. Yamamoto, Y. Ashida, and N. Kawakami, Rectification in nonequilibrium steady states of open many-body systems, Phys. Rev. Res. **2**, 043343 (2020).

[73] T. Jin, M. Filippone, and T. Giamarchi, Generic transport formula for a system driven by Markovian reservoirs, Phys. Rev. B **102**, 205131 (2020).

[74] T. Jin, J. S. Ferreira, M. Filippone, and T. Giamarchi, Exact description of quantum stochastic models as quantum resistors, Phys. Rev. Res. **4**, 013109 (2022).

[75] J. Ferreira, T. Jin, J. Mannhart, T. Giamarchi, and M. Filippone, Transport and nonreciprocity in monitored quantum devices: An exact study, Phys. Rev. Lett. **132**, 136301 (2024).

[76] A. M. Lacerda, J. Goold, and G. T. Landi, Dephasing enhanced transport in boundary-driven quasiperiodic chains, Phys. Rev. B **104**, 174203 (2021).

[77] F. Tonielli, R. Fazio, S. Diehl, and J. Marino, Orthogonality catastrophe in dissipative quantum many-body systems, Phys. Rev. Lett. **122**, 040604 (2019).

[78] M. T. Mitchison, T. Fogarty, G. Guarnieri, S. Campbell, T. Busch, and J. Goold, *In situ* thermometry of a cold Fermi gas via dephasing impurities, Phys. Rev. Lett. **125**, 080402 (2020).

[79] P. E. Dolgirev, J. Marino, D. Sels, and E. Demler, Non-Gaussian correlations imprinted by local dephasing in fermionic wires, Phys. Rev. B **102**, 100301(R) (2020).

[80] V. Alba, Unbounded entanglement production via a dissipative impurity, SciPost Phys. **12**, 011 (2022).

[81] S. Wolff, J.-S. Bernier, D. Poletti, A. Sheikhan, and C. Kollath, Evolution of two-time correlations in dissipative quantum spin systems: Aging and hierarchical dynamics, Phys. Rev. B **100**, 165144 (2019).

[82] Y. Li, X. Chen, and M. P. A. Fisher, Quantum Zeno effect and the many-body entanglement transition, Phys. Rev. B **98**, 205136 (2018).

[83] S. Choi, Y. Bao, X.-L. Qi, and E. Altman, Quantum error correction in scrambling dynamics and measurement-induced phase transition, Phys. Rev. Lett. **125**, 030505 (2020).

[84] M. J. Gullans and D. A. Huse, Dynamical purification phase transition induced by quantum measurements, Phys. Rev. X **10**, 041020 (2020).

[85] T. Müller, S. Diehl, and M. Buchhold, Measurement-induced dark state phase transitions in long-ranged fermion systems, Phys. Rev. Lett. **128**, 010605 (2022).

[86] J. C. Hoke, M. Ippoliti, E. Rosenberg, D. Abanin, R. Acharya, T. I. Andersen, M. Ansmann, F. Arute, K. Arya, A. Asfaw, *et al.*, Measurement-induced entanglement and teleportation on a noisy quantum processor, Nature (London) **622**, 481 (2023).

[87] I. Poboiko, P. Pöpperl, I. V. Gornyi, and A. D. Mirlin, Theory of free fermions under random projective measurements, Phys. Rev. X **13**, 041046 (2023).

[88] C. M. Caves and G. J. Milburn, Quantum-mechanical model for continuous position measurements, Phys. Rev. A **36**, 5543 (1987).

[89] D. Bernard, T. Jin, and O. Shpielberg, Transport in quantum chains under strong monitoring, Europhys. Lett. **121**, 60006 (2018).

[90] P. Das and S. Banerjee, Inverse superconductor-insulator transition in weakly monitored Josephson junction arrays, Phys. Rev. B **112**, L180503 (2025).

[91] J. Dalibard, Y. Castin, and K. Mølmer, Wave-function approach to dissipative processes in quantum optics, Phys. Rev. Lett. **68**, 580 (1992).

[92] H. J. Carmichael, *An Open Systems Approach to Quantum Optics*, Lecture Notes in Physics Vol. m18 (Springer, Berlin, 1993).

[93] V. P. Belavkin, in *Modeling and Control of Systems*, edited by A. Blaquiére (Springer, Berlin, 1989), pp. 245–265.

[94] H.-P. Breuer and F. Petruccione, *The Theory of Open Quantum Systems* (Oxford University Press, Oxford, 2002).

[95] A. Kamenev, *Field Theory of Non-Equilibrium Systems* (Cambridge University Press, Cambridge, 2011).

[96] A. I. Larkin and Y. N. Ovchinnikov, Nonlinear conductivity of superconductors in the mixed state, Sov. Phys. JETP **41**, 960 (1975).

[97] G. Del Pace, K. Xhani, A. Muzi Falconi, M. Fedrizzi, N. Grani, D. Hernandez Rajkov, M. Inguscio, F. Scazza, W. J. Kwon, and G. Roati, Imprinting persistent currents in tunable fermionic rings, Phys. Rev. X **12**, 041037 (2022).

[98] J.-P. Brantut, J. Meineke, D. Stadler, S. Krinner, and T. Esslinger, Conduction of ultracold fermions through a mesoscopic channel, Science **337**, 1069 (2012).

[99] S. Krinner, T. Esslinger, and J.-P. Brantut, Two-terminal transport measurements with cold atoms, J. Phys.: Condens. Matter **29**, 343003 (2017).

[100] B. Nagler, M. Will, S. Hiebel, S. Barbosa, J. Koch, M. Fleischhauer, and A. Widera, Ultracold Bose gases in dynamic disorder with tunable correlation time, Phys. Rev. Lett. **128**, 233601 (2022).

[101] S. Hiebel, B. Nagler, S. Barbosa, J. Koch, and A. Widera, Characterizing quantum gases in time-controlled disorder realizations using cross-correlations of density distributions, New J. Phys. **26**, 013042 (2024).